Available online at www.sciencedirect.com
SCIENCE DIRECT
Journal of Organometallic Chemistry 691 (2006) 1919–1926
Journal of Organometallic Chemistry
www.elsevier.com/locate/jorganchem

Solid-state *cis–trans* isomerization reaction of $(\eta^5\text{-MeC}_5\text{H}_4)\text{W(CO)}_2\text{P(O}^i\text{Pr)}_3\text{I}$

Muhammad D. Bala, Demetrius C. Levendis *, Neil J. Coville *

Molecular Sciences Institute, School of Chemistry, University of the Witwatersrand, 1 Jan Smuts Avenue, Private Bag 3, Johannesburg WITS 2050, South Africa

Received 30 November 2005; accepted 6 January 2006
Available online 20 February 2006

Abstract

cis-$(\eta^5\text{-MeC}_5\text{H}_4)\text{W(CO)}_2\text{P(O}^i\text{Pr)}_3\text{I}$ (**1**) was converted to the *trans* isomer **2** in the solid state (90–110 °C). The reaction was monitored by heating **1** in NMR tubes for periods of time (2–60 min), cooling the tubes to room temperature and determining the conversion by solution ^{31}P and ^{1}H NMR spectroscopy. The data were consistent with a first-order reaction and yielded an activation energy of 59 ± 3 kJ mol^{-1}. Comparative kinetic data were obtained from an in situ analysis of a powder-XRD study of **1**. The powder-XRD study was conducted at 80–100 °C (10–60 min), yielding an activation energy of 52 ± 2 kJ mol^{-1} (first-order reaction). The reaction could not be monitored by single crystal X-ray diffraction as the crystal disintegrated over time on heating. This disintegration process was monitored by optical microscopy and revealed that while the bulk crystal morphology was retained the crystal surface roughened with time. The compounds **1** and **2** were also structurally characterised by X-ray crystallographic techniques.

Keywords: Solid state chemistry; Melt reaction; Tungsten; *cis–trans* isomerisation

1. Introduction

Pseudo-seven coordinate four-legged piano stool complexes of the type RCpML_3X and RCpML_2X_2 (M = transition metal, L = 2 electron donor ligand and X = 1 electron donor ligand) have been well studied since their first syntheses in the 1950s [1]. The formation of their various isomeric forms is determined by the nature of the R, L and X groups [2]. Interest in these compounds stems from the facile inter-conversion of the different isomers. In general the *cis–trans* isomer inter-conversion processes are believed to occur via a Berry pseudo-rotation process or a turnstile mechanism involving two or three of the L and X ligands [3]. Further, these complexes are also useful for exploring many catalytic and non-catalytic reactions such as ligand substitution [4] and insertion reactions [5] which are mostly induced by thermal [6] and photochemical [7] techniques.

Recently, we have explored the isomerisation reaction of these pseudo-seven coordinate four-legged piano stool complexes in the solid and melt states [8]. In earlier work we showed that in general the solid state reaction occurred from the *trans* to the *cis* isomer for a wide range of complexes suggesting that the reaction direction may be determined by the electronic and steric factors associated with individual molecules [9]. However, the solid state isomerisation reaction of $(\eta^5\text{-MeC}_5\text{H}_4)\text{W(CO)}_2\text{P(O}^i\text{Pr)}_3\text{I}$ and $\{(\eta^5\text{-C}_5\text{Me}_5)\text{W(CO)}_2[\text{P(CH}_3)_3](\text{GeCl}_3)\}$ [10] are examples of reactions that proceed unidirectionally from the *cis* to the *trans* isomer. This suggests that the isomerisation reaction can also be influenced by the packing arrangement of the different isomers.

Other literature reports on related phenomena include: (i) attempts to isomerise *cis*-$(\eta^5\text{-C}_5\text{Me}_5)(\text{GeCl}_3)(\text{CO})_2\text{W=C(H)NEt}_2$ in the melt that resulted in the generation of a mixed isomer product [11]; and (ii) the observation

* Corresponding authors. Fax: +27 11 717 6749.
E-mail addresses: demi@hobbes.gh.wits.ac.za (D.C. Levendis), ncoville@aurum.chem.wits.ac.za (N.J. Coville).

0022-328X/$ - see front matter © 2006 Elsevier B.V. All rights reserved.
doi:10.1016/j.jorganchem.2006.01.014

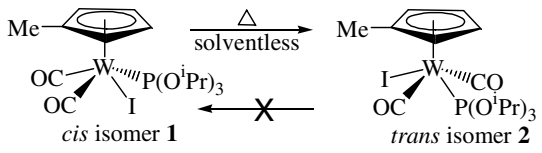

Scheme 1. Solid state *cis*-*trans* isomerization of **1** to **2**.

that the solid state isomerization of both *cis* and *trans* molybdenum piano-stool compounds can occur on standing to give a thermodynamic mixture, necessitating their storage at low temperatures [2c,12].

In this study we wish to report our comprehensive investigation on the *cis* to *trans* isomerisation reaction of (η^5-MeC$_5$H$_4$)W(CO)$_2$P(O^{i}Pr)$_3$I (Scheme 1), detailing a kinetic study of the isomerisation reaction using combined ^{1}H and ^{31}P NMR spectroscopy, PXRD and optical studies.

2. Results and discussion

2.1. Synthesis and spectroscopic data

The *cis* and *trans* isomers **1** and **2** were prepared by solution procedures. The reaction between P(O^{i}Pr)$_3$ and (η^5-MeC$_5$H$_4$)W(CO)$_3$I in CH_2Cl_2 produced **2** as the major product after 1 h of reaction at room temperature. Conversion to the *cis* isomer **1** was achieved by refluxing **2** in toluene (72 h). A search of the Cambridge Structural Database (CSD) [13] for pseudo-seven coordinate tungsten compounds with *cis*/*trans* piano-stool geometry have revealed that nearly 70% of all the compounds obtained (41 compounds) were isolated as the *trans* isomer. This may indicate that this is the more readily accessible isomer in solution.

The spectroscopic data on the two isomers, **1** and **2**, have been published earlier [14]. Further, characterization by ^{13}C NMR, ^{31}P NMR, powder and single crystal X-ray crystallography confirmed their structures and is discussed below.

A combination of infrared and NMR spectroscopic results revealed the geometry of each isomer in solution; this was confirmed by single crystal XRD studies. The IR spectra of the *cis* and *trans* isomers are easily distinguished by the relative intensities of the two ν(CO) absorptions. In **1**, the intensity of the symmetric CO stretching vibration at 1952 cm^{-1} is more intense than the antisymmetric CO stretching vibration at 1864 cm^{-1}, while in **2** it is the higher energy absorption at 1956 cm^{-1} that is less intense than the lower energy absorption at 1870 cm^{-1}.

The ^{31}P NMR spectra of **1** and **2** are characterised by singlets at 122 and 135 ppm, respectively, showing typical pair of satellites due to ^{183}W–^{31}P coupling. ^1J(W–P) coupling constants of 402.2 and 422.8 Hz measured for **1** and **2**, respectively is an indication that the tungsten metals in the two isomers are electronically similar. The ^{1}H NMR spectrum of the two isomers is characterised by an overlap of the Cp region between 5.12 and 5.36 ppm, and a similar overlap of the triisopropyl phosphite ligand region between 4.57 and 4.64 ppm further illustrating the electronic closeness of the two isomers. The ^{13}C NMR spectrum clearly confirms the configuration of the isomers **1** and **2**. In addition to the expected resonances for the Cp carbons and the triisopropyl phosphite carbons, two resonances are recorded for the two non-equivalent CO carbons of **1** at 227.6 and 241.9 ppm indicating a *cis* arrangement, while a single peak at 225.8 ppm was recorded for the two CO carbons of **2** as expected for an equivalent electronic environment in a *trans* configuration of a pseudo square-pyramidal complex.

For the purpose of establishing the identity of the isomers and their relative composition in a given sample, the ratio of the two ^{31}P peaks confirmed by the ratio of the Cp-Me protons peaks which are well separated in the ^{1}H spectra, were used.

2.2. Crystal structures

Numerical data relevant to the experimental measurement and details of the structure analyses are given in Table 1. The table shows that the crystal data for both isomers have a monoclinic structural configuration. The atomic numbering scheme for **1** and **2** are shown in the ORTEP diagrams (Figs. 1 and 2) where both **1** and **2** adopt a distorted square-pyramidal geometry. Selected bond lengths and angles are presented in Table 2. The bond lengths and angles of the two isomers are similar to what has been recorded for tungsten compounds containing similar ligand arrangements around the metal [14,15]. All the bond lengths are similar in the two isomers clearly in agreement with spectroscopic data (see above) and reveal the electronic similarity between the two isomers in spite of the differing *cis* and *trans* arrangements of the basal ligands around the W atom.

It is noteworthy that the diagonal angles around the tungsten atom indicate the influence of the ligand steric requirements on their spatial arrangement around the tungsten atom. In the *cis* isomer the two diagonal angles C(1)–W–I and C(2)–W–P are very close at 129° and 122°, respectively, while the corresponding angles in the *trans* isomer are C(1)–W–C(2) and I–W–P at 109° and 137°, respectively. In the square-pyramidal arrangement the MeCp ligands occupy the apical position yielding in the *cis* isomer a more regular arrangement of the four basal ligands. In the *trans* isomer the two sterically more demanding moieties, the triisopropylphosphite ligand and the iodide ion, occupy opposite positions of the basal corners of the distorted square with the CO ligands on the other corners.

More revealing are the crystallographic features from the crystal packing diagrams of **1** and **2** presented in Figs. 3 and 4. Adopting the "head" and "tail" terminology [14] to represent the cyclopentadienyl and phosphite moieties respectively, it can be seen that the packing arrangement in **1** is "head to head" through the first two adjacent rows

Table 1
Crystal data and structure refinement data for compounds **1** and **2**

Identification	**1**, *cis*	**2**, *trans*
Empirical formula	$C_{17}H_{28}IO_5PW$	$C_{17}H_{28}IO_5PW$
Formula weight	654.11	654.11
Temperature (K)	293(2)	293(2)
Wavelength (Å)	0.71073	0.71073
Crystal system, space group	Monoclinic, $P2_1/c$	Monoclinic, Cc
Unit cell dimensions		
a (Å)	17.912(5)	10.233(9)
b (Å)	8.564(5)	13.6590(13)
c (Å)	16.357(5)	16.356(16)
β (°)	114.731	100.740(10)
V (Å^3)	2279.0(16)	2246.1(4)
Z, D_{calc} (Mg/m^3)	4, 1.906	4, 1.934
Absorption coefficient (mm^{-1})	6.514	6.610
$F(000)$	1248	1248
Crystal size (mm)	$0.26 \times 0.24 \times 0.16$	$0.62 \times 0.44 \times 0.26$
Θ Range for data collection (°)	2.49–25.00	2.52–24.99
Limiting indices	$-21 \leqslant h \leqslant 19$, $-3 \leqslant k \leqslant 10$, $-18 \leqslant l \leqslant 19$	$-4 \leqslant h \leqslant 12$, $-14 \leqslant k \leqslant 16$, $-19 \leqslant l \leqslant 17$
Reflections collected/unique [R_{int}]	11403/3990 [0.0244]	5584/2472 [0.0251]
Completeness to $\Theta = 25.00$ (%)	99.6	99.5
Absorption correction	Empirical	Empirical
Max. and min. transmission	0.4221 and 0.2822	0.2783 and 0.1052
Refinement method	Full-matrix least-squares on F^2	Full-matrix least-squares on F^2
Data/restraints/parameters	3990/239/226	2472/240/233
Goodness-of-fit on F^2	1.071	1.140
Final R indices [$I > 2\sigma(I)$]	$R_1 = 0.0348$, $wR_2 = 0.0969$	$R_1 = 0.0218$, $wR_2 = 0.0558$
R indices all data	($R_1 = 0.0406$, $wR_2 = 0.1036$)	$R_1 = 0.0220$, $wR_2 = 0.0560$
Largest diff. peak and hole (e Å^{-3})	1.008 and −1.193	1.002 and −0.495

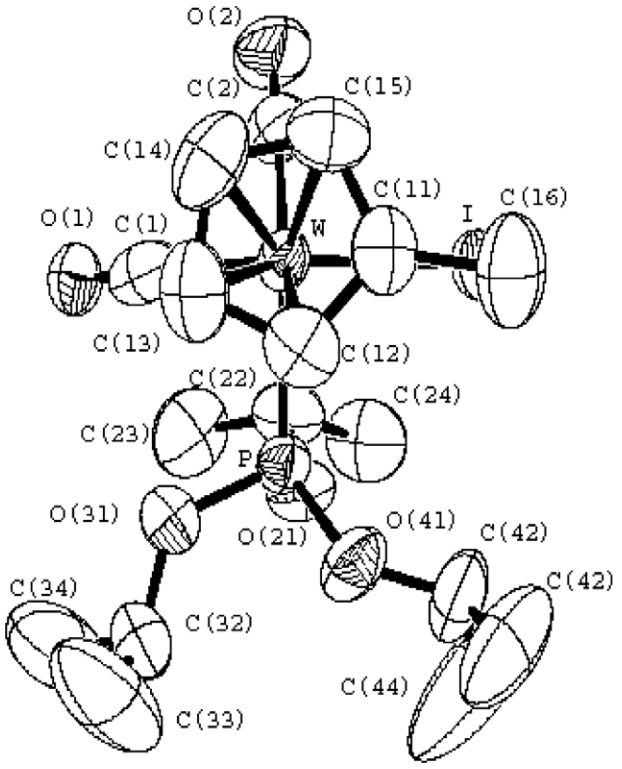

Fig. 1. ORTEP representation and numbering scheme of **1**. Thermal ellipsoids shown at 50% probability.

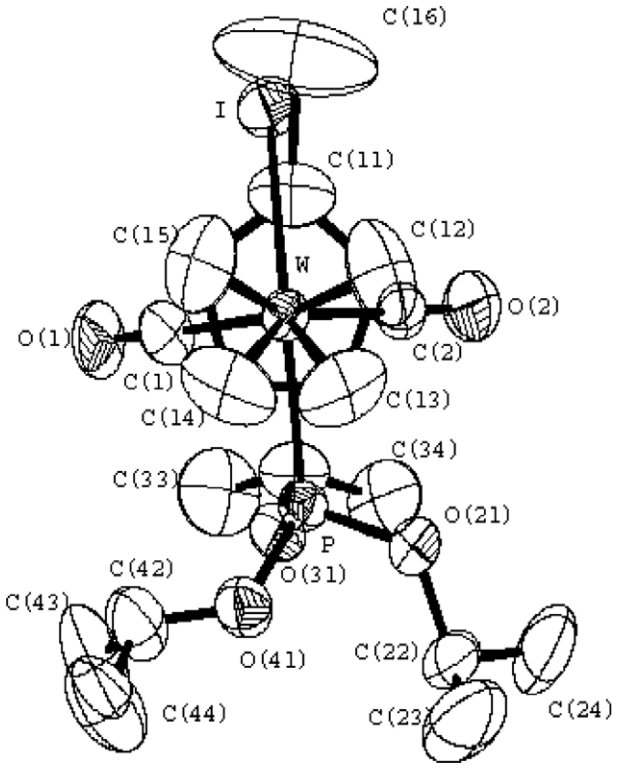

Fig. 2. ORTEP representation and numbering scheme of **2**. Thermal ellipsoids shown at 50% probability.

Table 2
Selected bond lengths (Å) and angles (°) for complexes **1** and **2**

Identification	**1**, *cis*	**2**, *trans*
W–C(2)	1.956(7)	1.966(8)
W–C(1)	1.989(8)	1.975(8)
W–P	2.4364(18)	2.395(2)
W–I	2.8343(6)	2.8343(7)
C(2)–W–C(1)	75.7(3)	109.5(3)
C(2)–W–P	121.8(3)	77.1(3)
C(1)–W–P	78.4(2)	79.5(3)
C(2)–W–I	76.9(3)	77.1(2)
C(1)–W–I	129.4(2)	77.1(2)
P–W–I	81.17(4)	136.71(5)
O(2)–C(2)–W	176.3(8)	173.1(7)
O(1)–C(1)–W	177.9(8)	174.9(8)

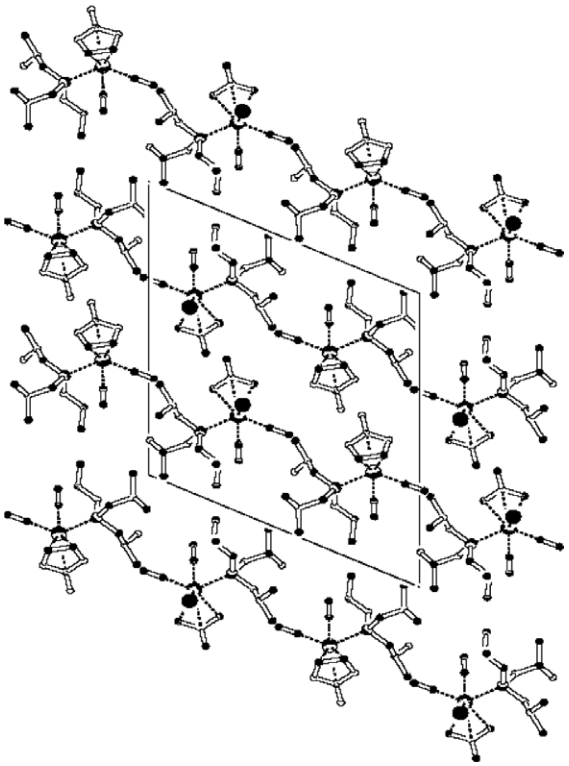

Fig. 3. Packing diagram of **1** viewed along the *b*-axis.

and "tail to tail" through the next. This yields an "open" arrangement in which the bulky MeCp rings and the iodide in one row sterically interact with those of the adjacent row and the corresponding phosphite ligands "interlocked" with those of the opposite row in the unit cell. This arrangement has two major implications for the mechanism of the *cis*-to-*trans* isomerisation reaction. The repulsive "head to head" arrangement creates voids that may serve to initiate the isomerisation reaction, while the interlocking "tail to tail" arrangement of the phosphite ligands may provide the axial anchor for the equatorial ligands to move in a combination Berry-turnstile rotation to complete a *cis–trans* transformation [3]. Conversely the packing arrangement in **2** is uniformly "head to tail" and in one orientation throughout the unit cell. This and the mild shrinkage in volume results in a higher density of **2** and may account for the unidirectional nature of the isomerization reaction being from **1** to **2**. In a control experiment (see below) no isomerization was observed when a sample of **2** was held above the melting points of **1** and **2** i.e. at 150 °C for 2 h (m.p., **2** = 144–146; m.p., **1** = 128–130 °C).

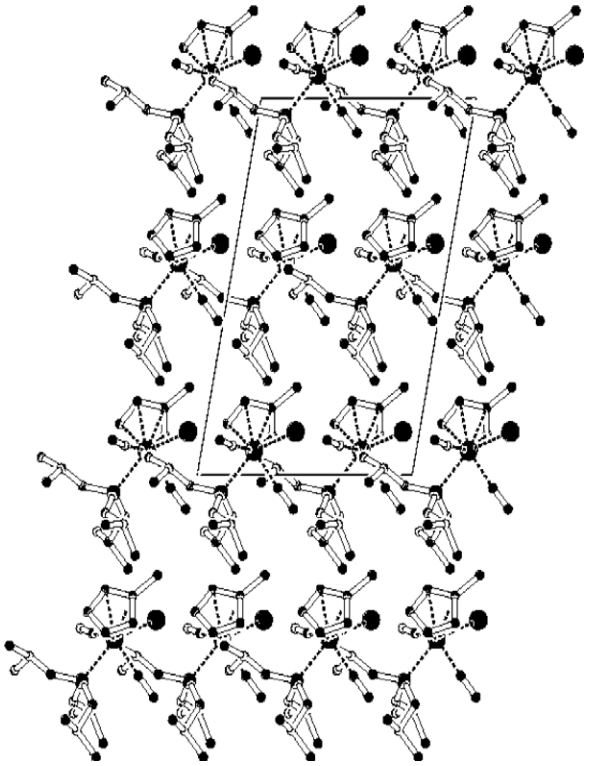

Fig. 4. Packing diagram of **2** viewed along the *b*-axis.

2.3. Solution isomerisation reaction

The synthetic route to the two isomers (see above) indicates that in solution the *trans* isomer is the kinetic product that is later thermally isomerised to the *cis* isomer. The product composition from the solution isomerisation reaction is also solvent dependant. For instance starting from the *trans* isomer a thermodynamic 50/50 *cis*/*trans* mixture is obtained in dichloromethane, while the equilibrium is tilted in favour of the *cis* isomer in refluxing toluene (>70%). Earlier solution phase isomerisation studies of a series of molybdenum and tungsten piano-stool complexes revealed the dependence of the direction and composition of the product on the solvent and the method of preparation [2c,16].

2.4. Melt isomerisation reaction

Literature data on melt-phase isomerisation of organometallic compounds are rare [10]. The few examples that have been reported have shown the versatility of this procedure as a means of preparing isomers that otherwise

are inaccessible via solution techniques. A melt study was carried out on the *trans* isomer **2**. The isomer was loaded into a dry and nitrogen purged NMR tube and heated to 150 °C in an oil bath and held at that temperature for 30 min. A comparison of the room temperature NMR patterns before and after the process confirmed that the solid/melt phase isomerisation is unidirectional and that no *trans–cis* transformation was observed. Gradual decomposition in the melt into an unidentified black solid was observed on extended heating (2 h) of **2** at 150 °C.

2.5. Kinetic studies of the solventless reactions

Kinetic information on the *cis–trans* isomerisation of **1** to **2** was obtained by a combination of ^{1}H NMR spectroscopy and PXRD analysis.

2.5.1. Kinetic studies monitored by ^{1}H NMR spectroscopy

In these experiments, the reactant, *cis* isomer was heated in an NMR tube, cooled, solvent added at room temperature and the rate of disappearance of its Cp-methyl peak (2.24 ppm) relative to that of the emergence of the Cp-methyl peak of the product, (*trans* isomer, 2.32 ppm) was monitored with time. It is worth noting that when pure **2** was heated to the melt under similar conditions (see above) no isomerisation was detected by ^{1}H NMR spectroscopy.

Fig. 5 shows a typical % conversion versus time curve for the *cis–trans* isomerisation reaction of **1** to **2** and a plot of ln (% *cis* isomer) versus time yielded a straight line curve typical of a first-order reaction (see supplementary material). From the plots, first-order rate constants of $6.04 \pm 1.75 \times 10^{-4}$, $1.26 \pm 0.5 \times 10^{-3}$, $1.75 \pm 0.54 \times 10^{-3}$ were calculated at 90, 100 and 110 °C respectively. An Arrhenius plot of the kinetic data yielded an activation energy of 59 ± 3 kJ mol^{-1}. This value may relate to either the actual isomerisation reaction of reactant molecules or to the movement of a reaction front within the solid state accompanied or followed by the molecular isomerisation reaction (see later). The value is to be compared with data obtained from other related solid state studies [(η^5-MeC_5H_4)$Mo(CO)_2P(O^iPr)_3I$ = 68 ± 10 kJ mol^{-1} [12] and (η^5-MeC_5H_4)$W(CO)_2PPh_3I$ > 160 kJ mol^{-1} [14], with both values being associated with *bidirectional* reactions.

2.5.2. Kinetic studies monitored by powder XRD

PXRD studies were performed to obtain kinetic data for the isomerisation reaction. The PXRD patterns of **1** and **2** (Fig. 6) reveal that the distinct peak at 5.47° in **1**, can be used to monitor the rate of conversion of **1** with time. By monitoring the disappearance of this peak, rate data were obtained at various temperatures. A typical pattern showing the gradual disappearance of the peak as the sample is heated in the aluminium block at 90 °C is represented in Fig. 7. The obtained data were analysed and converted to the percentage conversion of **1** with time. Again, % conversion versus time curve plots for the *cis*-to-*trans* isomerisation reaction of **1** to **2** and a plot of ln (% *cis* isomer) versus time yielded a straight line curve typical of a first-order reaction (plots in supplementary material). From the plots, first-order rate constants of $4.89 \pm 0.74 \times 10^{-4}$, $9.47 \pm 0.92 \times 10^{-4}$ and $1.25 \pm 0.31 \times 10^{-3}$ were obtained at 80, 90 and 100 °C respectively for the PXRD kinetics studies. An Arrhenius plot of the data yielded an activation energy of 52 ± 2 kJ mol^{-1}. This compares well with the data obtained for the ^{1}H NMR studies indicating that the PXRD technique can be used to monitor the kinetics of crystalline powdered materials. A similar correlation between ^{1}H NMR and PXRD kinetics data have been reported for the solid state isomerisation of six coordinate ruthenium complexes [17,18].

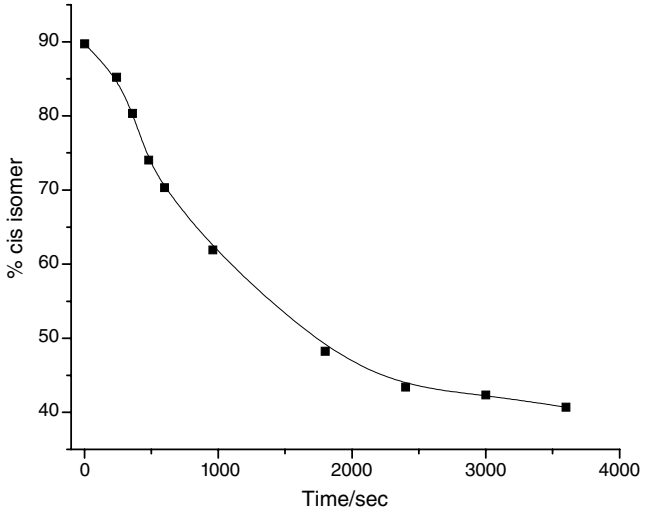

Fig. 5. Typical plot of data for the isomerization of **1** to **2** monitored by ^{1}H NMR spectroscopy.

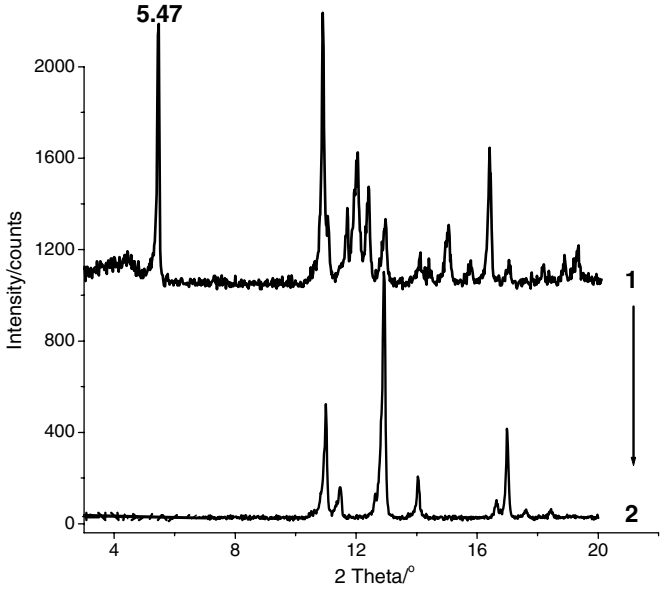

Fig. 6. Powder XRD patterns of **1** and **2** (note characteristic peak at 5.47°).

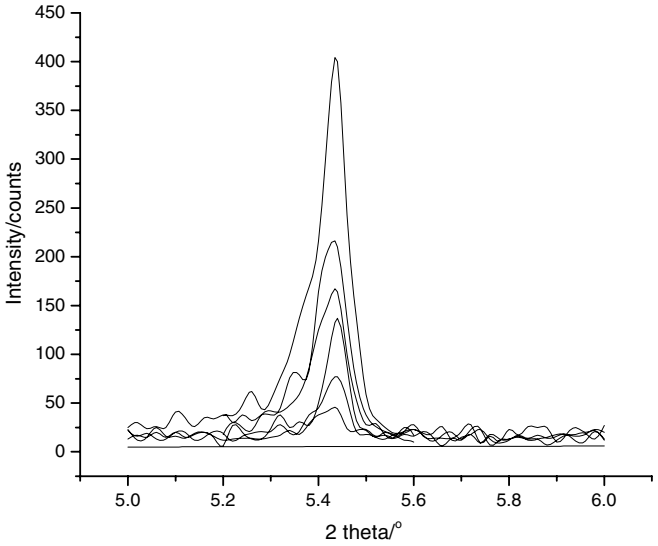

Fig. 7. Change in the PXRD pattern of **1** for the peak at 5.47° during the solid-state isomerization reaction at 90 °C.

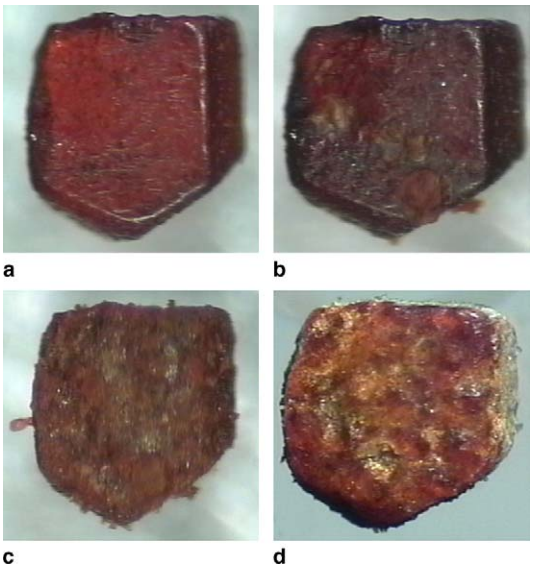

Fig. 8. Loss of crystallinity due to internal rupture in the isomerization of **1** to **2**. (a) Crystal of **1** at room temperature. (b) Same crystal held at 115 °C for 10 min. (c) Same crystal held at 115 °C for 30 min. (d) Same crystal held at 115 °C for 60 min. This gave powder rings on the SMART which resolved to a pattern similar to PXRD pattern of pure **2**.

2.6. Single crystal-to-crystal studies

Attempts to obtain a single crystal-to-crystal transformation of **1** to **2** were unsuccessful. When the reaction was monitored by single crystal studies the data revealed loss of crystallinity with time. This is connected with the supposed mechanism of the transformation from a *cis* to a *trans* conformation which is only possible by a loss of crystal geometry and generation of new geometry arrangements and packing. It was possible to monitor the changes in morphology with time under the optical microscope on heating a single crystal of **1**. At 115 °C, under a blanket of nitrogen the changes undergone by **1** were recorded by a digital camera mounted on a polarising microscope and are shown in Fig. 8. The pictures show that in the initial stages of heating (10 min) the crystal of **1** changed colour (became darker) while at the same time the surface started to roughen (Fig. 8b). The surface roughening effect could be due to: (i) a localised solid-liquid-solid transformation; or (ii) a bulk mediated process in which internal stresses induce surface effects. The build up of internal stresses would be brought about by the concerted movement of ligands in the isomerisation reaction. These stresses would lead to the surface effects observed. Similar observations have been described by Kaupp for a range of organic systems [19]. The progress of the reaction was monitored for 1 h with pictures taken at 10 min intervals which all showed the gradual progress of the roughening process that eventually engulfed the entire body of the crystal (Fig. 8c). Although not homogeneous, the external morphology of the crystal was retained at all times (Fig. 8d). The loss in crystallinity was also clear from the opaque appearance of the product. Crystal XRD analysis of the product revealed only powder rings that resolved to give patterns similar to the direct powder XRD pattern for pure **2** (obtained by crystallisation). This suggests that the product formed in the reaction is identical to that formed by crystallisation from solution of CH_2Cl_2/hexane, indicating that **2** has the same polymorphic structure when obtained from either source. The simulated powder pattern obtained from a single crystal of **2** was also identical to the powder pattern obtained by thermally converting **1** to **2**.

From the data described above it can readily be deduced that **1** transforms into **2** in the absence of solvents. While little can be said about intermediates in the process, **2** must be the thermodynamic sink in this solvent-free reaction (solid state or melt phase). In an attempt to rationalise the above observations an analysis of the single crystal structures was undertaken. Platon plots of the crystal packing in **1** and **2** (similar to Figs. 3 and 4) indicates the presence of voids between molecules in the packing of **1**, which are clearly absent in the packing of **2**. The presence of the voids may allow for free ligand motion and ultimately isomerisation. With reference to an analysis of the 41 tungsten compounds obtained from a CSD [13] search, a Platon analysis for voids indicated a majority (27 compounds, 66%) contained voids of various shapes and configurations. However, only two pairs of compounds have been subjected to solid state isomerization studies. These compounds with CSD codes GISNEB and GISNIF {(η^5-C_5Me_5)$W(CO)_2$[$P(CH_3)_3$]($GeCl_3$)} [10]; and IZUTEC and IZUTIG (η^5-MeC_5H_4)$W(CO)_2PPh_3I$ [14] show that the presence of voids is not a precondition for isomerization.

3. Conclusion

Kinetic data have been obtained for the isomerisation reaction of **1** to **2**. This data together with X-ray and optical data are consistent with a first-order reaction that

shows a clean uni-directional conversion to product. The optical data are also consistent with a reaction occurring at a melt front. As a consequence the information does not establish as to whether the kinetic data refer to the actual molecular isomerisation process or to the movement of the reaction front.

Finally, it is to be noted that our many attempts to use molecular mechanics calculations to rationalise the isomerisation reaction have not been successful. Indeed calculations continue to give the reverse direction from that observed experimentally. Clearly the force fields currently available for the calculation need revision.

4. Experimental

4.1. Synthesis

All operations involving the handling of air sensitive materials were carried out under dry nitrogen using standard Schlenk techniques or a glove box. Solvents were dried by conventional methods and distilled under nitrogen prior to use.

4.2. cis-(1) and trans-(2) (η^5-MeC_5H_4)$W(CO)_2P(O^iPr)_3I$

A generalised synthetic methodology to the title complexes *cis* (**1**) and *trans* (**2**) (η^5-MeC_5H_4)$W(CO)_2P(O^iPr)_3I$ following the procedure of Blumer et al. [4b] has been published elsewhere [14]. In the present report, a modification of the earlier procedure was employed in order to avoid isomer mixtures and the problems associated with their separation. The reaction of (η^5-MeC_5H_4)$W(CO)_3I$ with an excess of the ligand $P(O^iPr)_3$ and trimethylamine *N*-oxide in dichloromethane at room temperature was monitored by infrared spectroscopy and was terminated within the first 1 h of reaction to give exclusively *trans* product in quantitative yield (>90%). Longer reaction times resulted in the formation of isomer mixtures, and a 50/50 *cis*/*trans* mixture was usually obtained in dichloromethane after 24 h [14]. Solution phase isomerisation of the *trans* product in refluxing toluene for 72 h gave a good yield (>70%) of the *cis* product.

4.3. X-ray structure determination and refinement

Crystallographic data were collected on a Bruker SMART 1 K CCD area detector diffractometer with graphite monochromated Mo Kα radiation (50 kV, 30 mA). The collection method involved ω-scans of width 0.3°. Numerical data pertaining to the experimental measurement and details of the structure analyses are given in Table 1. Data reduction were carried out using the program SAINT+ [20] and data were corrected for absorption using the program SADABS [20]. The structures were solved by standard Patterson procedures and refined by least-squares methods based on F^2. The SHELX [21] suite of programs as incorporated into WINGX [22] was used for all crystallographic computations. In the final stages of refinement hydrogen atoms were geometrically fixed and allowed to ride on the respective atoms.

4.4. Kinetic studies

Kinetics data were obtained for the solid state isomerization reaction of **1** to **2** by ^{1}H NMR spectroscopy and by powder XRD procedures. Attempts to obtain single-to-single crystal XRD kinetics data were unsuccessful due to the disruption of crystallinity as sample heating progressed.

4.4.1. ^{1}H NMR kinetic experiments

About 5–10 mg of the sample **1** was put in NMR tubes purged with N_2 and placed in an oil bath at a preset temperature. Data were collected by removing a tube at a required time interval, chilling it in ice, dissolving the sample in a known amount of chloroform, and immediately recording the NMR spectrum on a Bruker AC300 NMR spectrometer operating at 300 MHz.

4.4.2. Powder XRD kinetic experiments

A modified sample holder made from a standard aluminium sheet containing a machined capillary-size pouch, 2 mm wide × 15 mm long, was used for sample analysis and data acquisition. The aluminium PXRD cell was packed with finely ground powdered sample and enclosed in an aluminium heating block built for this study. The block is equipped with nitrogen inlets and outlets that allow for working under an inert atmosphere up to a temperature of 200 °C. The sample was loaded for PXRD measurement and the first measurement at time zero and room temperature was recorded. The loaded sample holder was then placed in the heating block and heating was commenced and the sample maintained at required temperatures for a set time interval. Data were collected by removing the cell at time intervals, draining away heat from the reaction cell and measuring the PXRD intensity from $2\Theta = 5$–6° at room temperature on a Philips PW 1710 diffractometer.

The PXRD patterns of **1** and **2** are presented in Fig. 6. The PXRD diffraction pattern for **1** shows a distinct peak at 5.47°. The rate of disappearance of this peak (Fig. 7) was followed with time to obtain kinetic data that fitted a first-order plot (see supplementary material Fig. S3). The main advantage of this method is that the same sample was used throughout a single experiment. Therefore variations in sample packing depth and surface changes associated with multiple sample packing are eliminated. Also, it was much easier to achieve a near uniform surface packing of the sample, due to the small capillary size of the sample containment pouch. All these effects combined to generate reproducible and reliable kinetic data.

4.5. Optical microscopic study

The apparatus used to monitor single crystals by optical microscopy has been described previously [17]. A single

crystal of **1** was placed on a transparent glass slide containing a thermocouple and the slide loaded into an enclosed chamber containing the aluminum heating block. The cell was then purged with nitrogen. The cell was mounted under a polarizing microscope equipped with a digital camera. At intervals digital images of the physical changes occurring on the surface of the crystal, as it was being heated, were recorded. To avoid sample oxidation a gentle flow of nitrogen was maintained through the cell over the course of the experiment.

Acknowledgements

We thank the NRF, THRIP, and the University of the Witwatersrand for financial support.

Appendix A. Supplementary data

First-order plots for the conversion of **1** to **2** monitored by ^{1}H NMR and by PXRD are available. Also, crystallographic data for the structural analysis has been deposited with the Cambridge Crystallographic Data Centre, CCDC Nos. 275755 and 275756 for compounds **1**, and **2**, respectively. Copies of this information may be obtained free of charge from: The Director, CCDC, 12 Union Road, Cambridge, CB2 1EZ UK, fax: +44(1223)336-033, or email: deposit@ccdc.cam.ac.uk or www: http://www.ccdc.cam.ac.uk. Supplementary data associated with this article can be found, in the online version, at doi:10.1016/j.jorganchem.2006.01.014.

References

[1] (a) T.S. Piper, G. Wilkinson, J. Inorg. Nucl. Chem. 3 (1956) 104;
(b) R.B. King, Inorg. Chem. 2 (1963) 936;
(c) M.J. Bennet, R. Mason, Proc. Chem. Soc. London (1963) 273;
(d) J.B. Wilford, A. Whitla, H.M. Powell, J. Organomet. Chem. 8 (1967) 495;
(e) F.A. Cotton, M.D. LaPrade, J. Am. Chem. Soc. 90 (1968) 5418;
(f) M.R. Churchill, J.P. Fennessey, Inorg. Chem. 7 (1968) 953;
(g) M.J. Morris, in: E.W. Abel, F.G.A. Stone, G. Wilkinson (Eds.), Comprehensive Organometallic Chemistry, vol. 5, Pergamon Press, New York, 1995, p. 407.

[2] (a) R.B. King, R.H. Reimann, D.J. Darensbourg, J. Organomet. Chem. 93 (1975) C23;
(b) D.L. Bleach, K.W. Barnett, J. Organomet. Chem. 97 (1975) C27;
(c) D.L. Bleach, M. Dattilo, K.W. Barnett, J. Organomet. Chem. 140 (1977) 47.

[3] (a) J.W. Faller, A.S. Anderson, J. Am. Chem. Soc. 91 (1969) 1550;
(b) J.W. Faller, A.S. Anderson, J. Am. Chem. Soc. 92 (1970) 5852;
(c) T.C. Flood, E. Rosenberg, A. Sarhangi, J. Am. Chem. Soc. 99 (1977) 4334;
(d) E. Pfeiffer, K. Vrieze, J.A. McCleverty, J. Organomet. Chem. 174 (1979) 183;
(e) J.M. Smith, N.J. Coville, Organometallics 15 (1996) 3388.

[4] (a) A.R. Manning, J. Chem. Soc. (A) (1967) 1984;
(b) D.J. Blumer, K.W. Barnett, T.L. Brown, J. Organomet. Chem. 173 (1979) 71;
(c) T.Y. Luh, Coord. Chem. Rev. 59 (1984) 225.

[5] (a) I.S. Butler, F. Basolo, R.G. Pearson, Inorg. Chem. 6 (1967) 2074;
(b) J.D. Cotton, G.T. Crisp, V.A. Daly, Inorg. Chim. Acta 47 (1981) 165;
(c) K.W. Barnett, D.L. Beach, S.P. Gaydos, T.G. Pollmann, J. Organomet. Chem. 69 (1974) 121;
(d) O.G. Adeyemi, N.J. Coville, Organometallics 22 (2003) 2284;
(e) M.D. Bala, A. Budhai, N.J. Coville, Organometallics 23 (2004) 2048.

[6] (a) P.M. Treichel, K.W. Barnett, R.L. Shubkin, J. Organomet. Chem. 7 (1967) 449;
(b) K. Starker, M.D. Curtis, Inorg. Chem. 24 (1985) 3006;
(c) J. Febway, F. Casabianca, J.G. Riess, Inorg. Chem. 24 (1985) 3235.

[7] (a) D.G. Always, K.W. Barnett, Inorg. Chem. 19 (1980) 1533;
(b) R.H. Hill, J.D. Debad, Polyhedron 10 (1991) 1705;
(c) J.D. Debad, R.H. Hill, Can. J. Chem. 68 (1990) 2216;
(d) W. Xia, R.H. Hill, Polyhedron 11 (1992) 1319;
(e) L. Cheng, N.J. Coville, Organometallics 16 (1997) 591.

[8] (a) N.J. Coville, L. Cheng, J. Organomet. Chem. 571 (1998) 149;
(b) N.J. Coville, D.C. Levendis, Eur. J. Inorg. Chem. (2002) 3067.

[9] (a) L. Cheng, N.J. Coville, Organometallics 15 (1996) 867;
(b) L. Cheng, N.J. Coville, J. Organomet. Chem. 556 (1998) 111;
(c) L. Cheng, L. Carlton, N.J. Coville, S. Af. J. Chem. 51 (1998) 127;
(d) R.S. Bogadi, D.C. Levendis, N.J. Coville, J. Am. Chem. Soc. 124 (2002) 1104.

[10] A.C. Fillippou, J.G. Winter, M. Feist, G. Kociok-Köhn, I. Hinz, Polyhedron 17 (1998) 1103.

[11] A.C. Fillippou, P. Portius, J.G. Winter, G. Kociok-Köhn, J. Organomet. Chem. 628 (2001) 11.

[12] O.G. Adeyemi, M.A. Fernandes, L. Cheng, U.B. Eke, D.C. Levendis, N.J. Coville, C.R. Chimie 5 (2002) 387.

[13] CSD ConQuest 1.6, Version 5.26 (February 2005 updates): I.J. Bruno, J.C. Cole, P.R. Edgington, M. Kessler, C.F. Macrae, P. McCabe, J. Pearson, R. Taylor, Acta Crystallogr. B 52 (2002) 389.

[14] O.G. Adeyemi, U.B. Eke, L. Cheng, L.M. Cook, D.G. Billing, B.B. Mamba, D.C. Levendis, N.J. Coville, J. Organomet. Chem. 689 (2004) 2207.

[15] (a) D.G. Billing, N.J. Coville, J. Lesia, M.D. Bala, Acta Crystallogr., Sect. E: Struct. Rep. Online 60 (2004) m477;
(b) J.A.K. Howard, J.C. Jeffery, J.C.V. Laurie, I. Moore, F.G.A. Stone, A. Stringer, Inorg. Chim. Acta 100 (1985) 23;
(c) N.N. Turaki, J.M. Huggins, L. Lebioda, Inorg. Chem. 27 (1985) 424;
(d) H. Adams, N.A. Bailey, G.W. Bentley, G. Hough, M.J. Winter, S. Woodward, J. Chem. Soc., Dalton Trans. (1991) 749;
(e) H.A. Adams, N.A. Bailey, J.T. Gauntlett, I.M. Harkin, M.J. Winter, S. Woodward, J. Chem. Soc., Dalton Trans. (1991) 1117;
(f) M.I. Bruce, M. Ke, P.J. Low, B.W. Skelton, A.H. White, Organometallics 17 (1998) 3539.

[16] L. Cheng, Ph.D. Thesis, University of the Witwatersrand, Johannesburg, 1998.

[17] O.P.M. Horwood, D.G. Billing, D.C. Levendis, F.M. Nareetsile, N.J. Coville, Cryst. Eng. Commun. 5 (2003) 468.

[18] F.M. Nareetsile, O.P.M. Horwood, D.G. Billing, D.C. Levendis, N.J. Coville, J. Organomet. Chem. 682 (2003) 2.

[19] G. Kaupp, in: J.L. Atwood, J.E.D. Davies, D.D. MacNicol, F. Votgle (Eds.), Comprehensive Supramolecular Chemistry, vol. 8, Pergamon Press, New York, 1996 (Chapter 9).

[20] SAINT+, Version 6.02 (includes XPREP and SADABS), Bruker AXS Inc., Madison, WI, 1999.

[21] G.M. Sheldrick, SHELX 97 (includes SHELXS 97, SHELXL 97 and CIFTAB), Programs for Crystal Structure Analysis (Release 97-2), University of Göttingen, Germany, 1997.

[22] L.J. Farrugia, J. Appl. Cryst. 32 (1999) 837.